Supporting Information

A single-gold-atom addition regulates sharp redshift in fluorescence of atomically precise nanoclusters

Yesen Tan,[‡a,b] Kang Li,[‡c] Jingjing Xu,[b] Qinzhen Li,[b] Sha Yang,[b] Jinsong Chai,*[b] Yong Pei,*[c] Dianzeng Jia,*[a] and Manzhou Zhu*[b]

[a] Y. Tan, Prof D. Jia
Key Laboratory of Energy Materials Chemistry, Ministry of Education, Key Laboratory of Advanced Functional Materials, Autonomous Region, Institute of Applied Chemistry, Xinjiang University, Urumqi, Xinjiang 830046 (China)
E-mail: jdz@xju.edu.cn

[b] Y. Tan, Dr. Q. Li, Prof. S. Yang, Dr. J. Chai, Prof. M. Zhu
Department of Chemistry and Centre for Atomic Engineering of Advanced Materials, Key Laboratory of Structure and Functional Regulation of Hybrid Materials of Ministry of Education, Institutes of Physical Science and Information Technology and Anhui Province Key Laboratory of Chemistry for Inorganic/Organic Hybrid Functionalized Materials, Anhui University, Hefei, Anhui 230601 (China)
E-mail: chaijs@ahu.edu.cn; zmz@ahu.edu.cn

[c] K. Li, prof. Y. Pei
Department of Chemistry, Key Laboratory of Environmentally Friendly Chemistry and Applications of MOE, Xiangtan University, Xiangtan, Hunan 411105 (China)
Email: ypnku78@gmail.com

[‡] These authors contributed equally to this work.

Table of Contents

1. Experimental Procedures

1.1 Materials

All the solvents and reagents used in this study were commercially available and used as received without further purification. Dichloromethane (DCM, HPLC grade), Dichloromethane ($CDCl_3$, HPLC grade), methanol (MeOH, HPLC grade), toluene (HPLC grade), *n*-hexane (*n*-Hex, HPLC grade), 4-tert-butylphenylthiophenol (TBBT, ≥98%), triphenylphosphine (TPP, ≥98%), $HAuCl_4 \cdot 4H_2O$ (≥99.99%, metals basis) and sodium borohydride ($NaBH_4$, ≥98%) were all purchased from Shanghai Aladdin Bio-Chem Technology CO., Ltd. The ultrapure water (≥18.2 MΩ) used in this study was purified on a Millipore system (Millipore, USA). All glassware was washed with aqua regia and rinsed with ultrapure water prior to use.

1.2 Synthesis and purification of the Au_{37} nanocluster.

Au_{37} has two synthetic strategies, which are method I and method II.

In **method I**, the Au_{37} nanocluster was synthesized using a one-pot and size-focusing synthesis strategy, which is a similar method reported for the synthesis of Au_{36},[1] but with extra phosphine ligands. Typically, $HAuCl_4 \cdot 4H_2O$ (82.4 mg, 0.20 mmol) was dissolved in 5 mL water, and TOAB (150 mg, 0.28 mmol) was dissolved in 15 mL dichloromethane. These two solutions were combined in a 25 mL tri-neck round bottom flask. The solution was vigorously stirred (~1100 rpm) with a magnetic stir bar to facilitate the phase transfer of Au(III) salt into the organic phase. After ~15 min, phase transfer was completed and the aqueous was then removed. After that, 4-tert-butylphenylthiophenol (150 µL, 0.90 mmol) and PPh_3 (15 mg, 0.057 mmol) were added into the above solution order, and the color of the solution changed to colorless. After ~ 30 min, 3 mL aqueous solution of $NaBH_4$ (77 mg, 2.03 mmol) was added slowly. Then, the reaction was allowed to proceed for ~12 h. The product was washed several times with CH_3OH to remove the excess ^{t}BuPhSH, PPh_3, and by-products. Then, the crude product was extracted with CH_2Cl_2 twice. The crude product was then re-dissolved in 3 mL of toluene and reacted with 100 µL of ^{t}BuPhSH under 80 °C. After reacting for 12 h, the product was washed with methanol several times and further purified by thin-layer chromatography (TLC, DCM: n-hexane= 1 : 2). The raw product containing Au_{37} was loaded on TLC plates for purification with a yield of about 2.95% (1.80 mg) based on the gold.

In **method II**, Pure Au_{36} (20 mg) was used as a precursor by reacting with pre-prepared gold-phosphine complexes (Ph_3P)AuCl (1 mg, ~1 equivalent) and the reaction was allowed to proceed overnight. (Ph_3P)AuCl was prepared by mixing $HAuCl_4 \cdot 4H_2O$ (20.6 mg, 0.05 mmol) with PPh_3 (26.2 mg, 0.10 mmol) in ethanol solution ($HAuCl_4 + H_2O + 2\ PPh_3 \rightarrow (Ph_3P)AuCl + Ph_3PO + 3\ HCl$) and washed three times with ethanol to remove the excess impurity. The purification of the targeted Au_{37} nanocluster was performed by thin layer chromatography with DCM/n-hexane (v:v = 1 : 2) as developing solvent. The raw product containing Au_{37} was loaded on TLC plates for purification with a yield of about 5.49% (1.03 mg) based on Au_{36}.

1.3 X-ray Crystallographic Determination.

Single crystal X-ray diffraction (SCXRD) of it was carried out on a Stoe Stadivari diffractometer at 293 K, using a Cu Kα radiation (λ = 1.54186 Å) for Au_{37}. The structure

was solved by direct methods and refined with full-matrix least-squares on F^2 using the SHELXL-2014/7 (Sheldrick, 2014) suite of programs. All the refinement parameters are summarized in Table S2.

1.4 Computational method and details

Both DFT calculations and TDDFT calculations were done using ORCA5.0.2 software[2]. The geometric optimization of the ground and excited states of the gold clusters was carried out using the PBE0 exchange-correlation functional[3] and the def2-SV(P) basis set. To improve the computational efficiency, both DFT and TDDFT calculations were performed using the RI (Resolution of Identity) approximation with the auxiliary basis set def2/J[4]. To facilitate the calculation, we simplified the thiol ligand Bu^{t}PhSH and phosphine ligand Ph_3P to CH_3SH and $(CH_3)_3P$. All structures were optimized in the gas phase. The convergence criteria for geometric optimization are set as 1.0×10^{-6}Hartree for energy change and 3.0×10^{-4}Hartree/Å for gradient change, respectively. The geometric optimization of the S_0 is performed by using DFT method, and the structural optimization of S_1 is performed using TDDFT method. Vertical excitation energy and Vertical emission energy are calculated at the optimized ground state S_0 and excited-state S_1 structures, respectively.

Based on the results of optimized S_0 and S_1 by ORCA5.0.2, the wave function information of hole and electron pairs were obtained by calculating TDDFT single point energy at PBE0/def2-SVP level with Gaussian 09 program[5], and then electron-hole[6] and inter fragment charge transfer (IFCT)[7] analysis were performed using Multiwfn 3.8 (dev) program[8].

1.5 Characterization.

UV-vis absorption spectra were recorded on an Agilent 8453 spectrophotometer. Fluorescence spectra were obtained using an F-7000 fluorescence spectrophotometer. X-ray photoelectron spectroscopy (XPS) measurements were performed on a thermal ESCALAB 250, equipped with a monochromated Al Kα (1486.8 eV) 150 W X-ray source, 0.5 mm circular spot size, and a flood gun (to counter charging effects). The analysis chamber base pressure was lower than 1×10^{-9} mbar, and data were collected with FAT = 20 eV. Electrospray ionization mass spectra (ESI-MS) were recorded using a Waters Xevo G2-XS mass spectrometer. The source temperature was maintained at 80 °C. The sample was directly infused into the chamber at 5 µL/min. ESI sample was prepared by dissolving it in dichloromethane/methanol (0.1 mg/mL). NIR emission was taken in an edinburgh instruments FS5 Spectrophotometer. QY of the nanoclusters in this work was estimated using Au_{25} as a reference.[9]

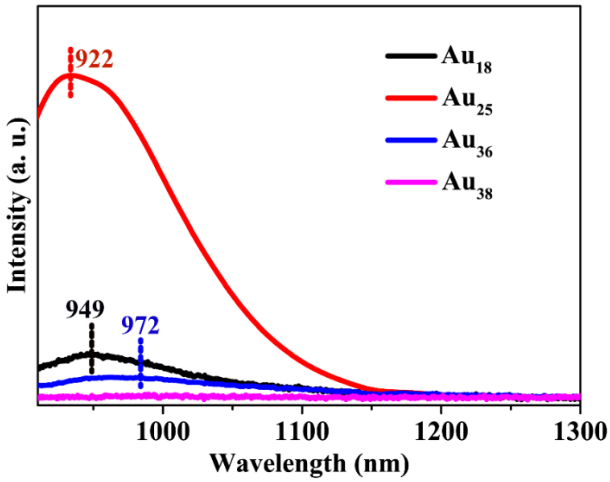

Figure S1. Near-infrared fluorescence emission wavelength measurements of Au_{18}(S-*c*-C_6H_{11})$_{14}$, Au_{25}(PET)$_{18}$, Au_{36}(TBBT)$_{24}$ and Au_{38}(PET)$_{24}$ nanoclusters.

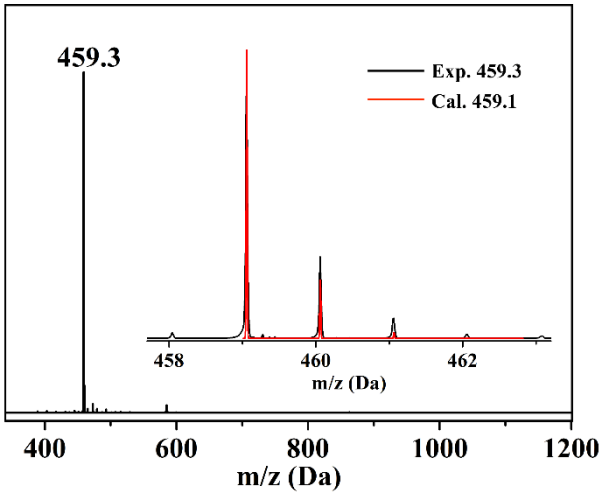

Figure S2. ESI-MS of [(Ph_3P)AuCl], interpolation is experimental and theoretical simulation. The m/z peak at 459.3 is [(Ph_3P)Au]$^+$, which is formed by the [(Ph_3P)AuCl] molecule losing a Cl atom.

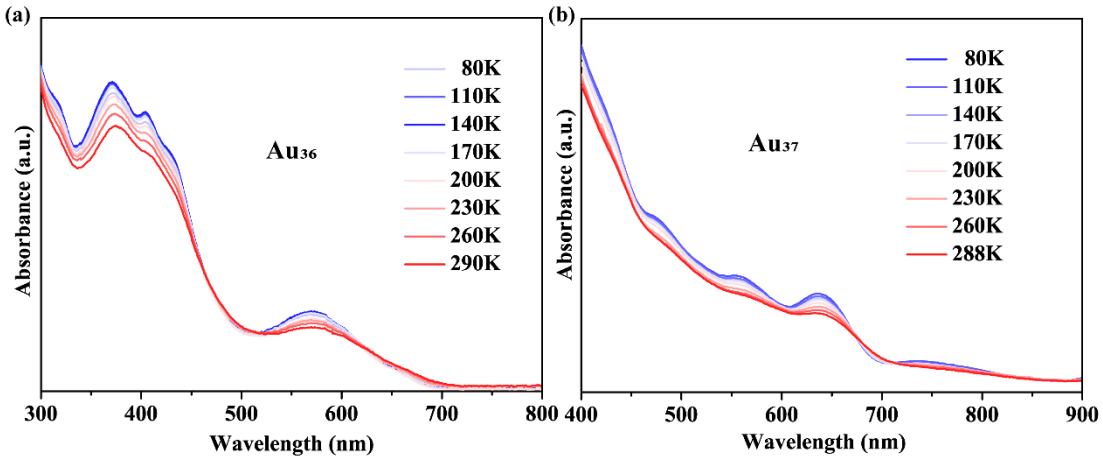

Figure S3. Temperature-dependent UV-vis absorption spectra of (a) Au_{36} and (b) Au_{37} nanoclusters.

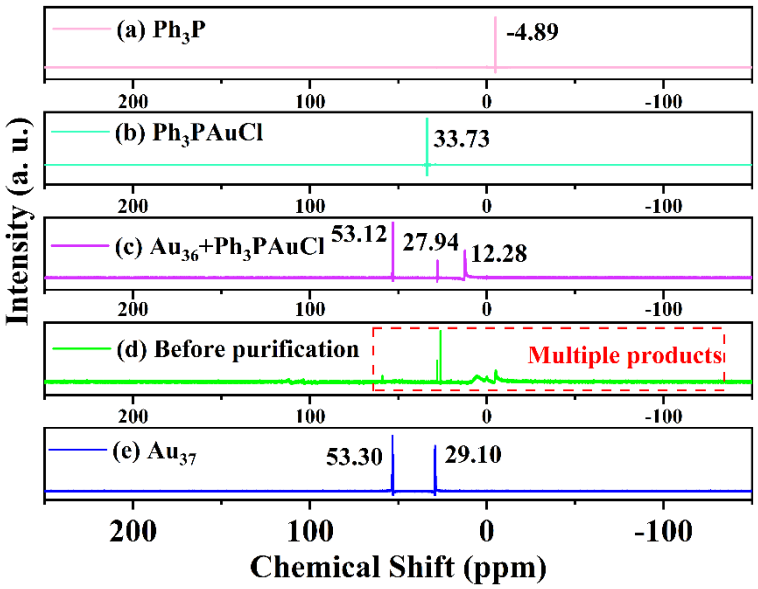

Figure S4. The ^{31}P NMR spectra of (a) TPP, (b) reaction process and (c) Au_{37} nanocluster.

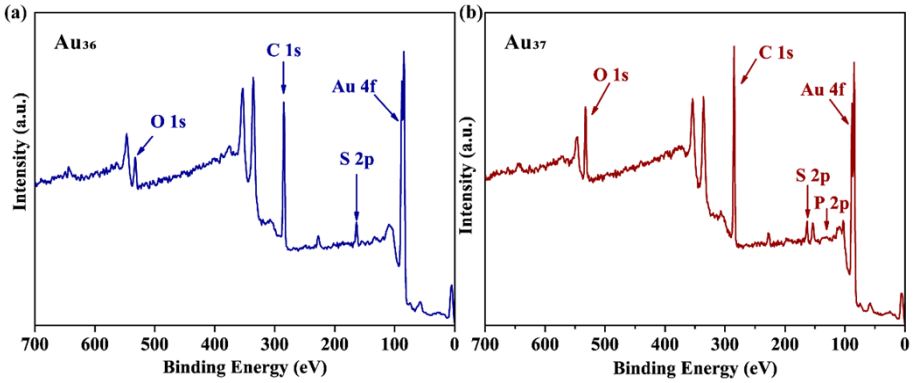

Figure S5. Full X-ray photoelectron spectroscopy (XPS) of (a) Au_{36} and (b) Au_{37} nanoclusters.

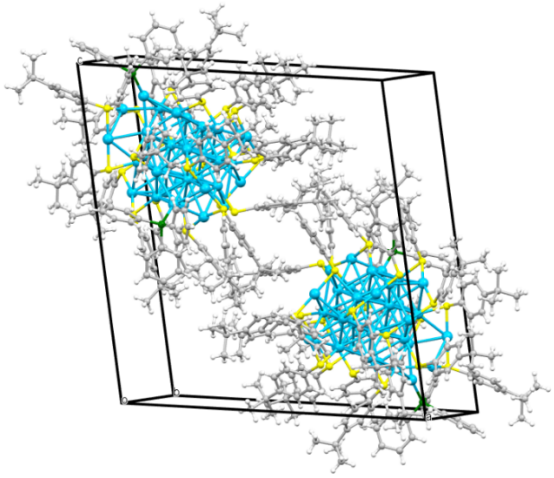

Figure S6. Unit cells of Au_{37} nanocluster (color coded: Au = blue; S = yellow; P = green; C = gray; H = white).

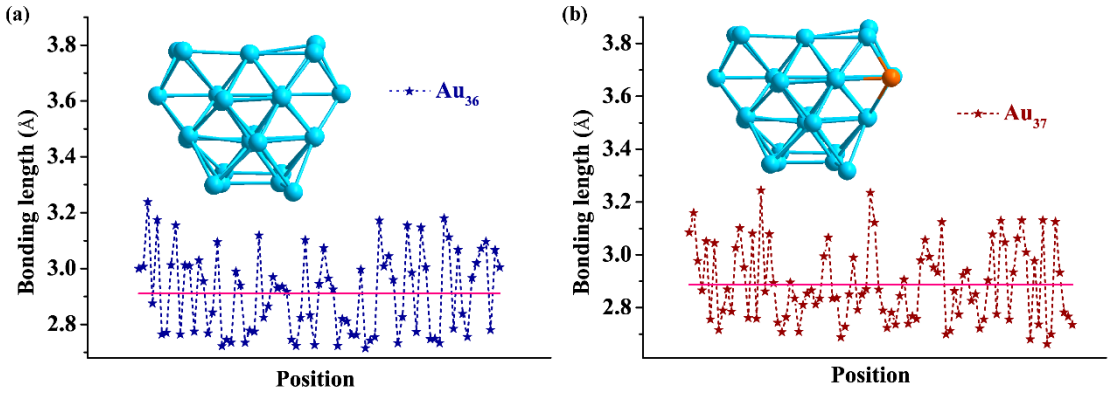

Figure S7. Kernel Au-Au bond length statistics of (a) Au_{36} and (b) Au_{37} nanoclusters.

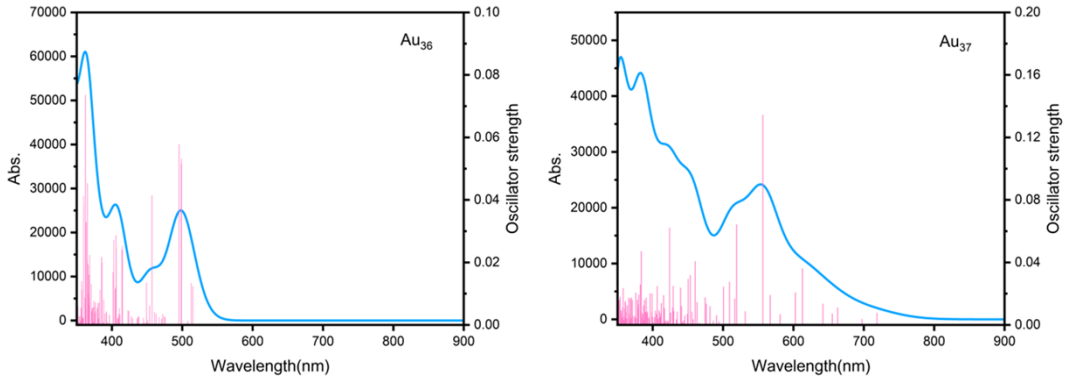

Figure S8. The calculated absorption spectra of Au_{36} and Au_{37} at TD DFT are compared with the experimental spectra (PBE0/def2-SV(P)).

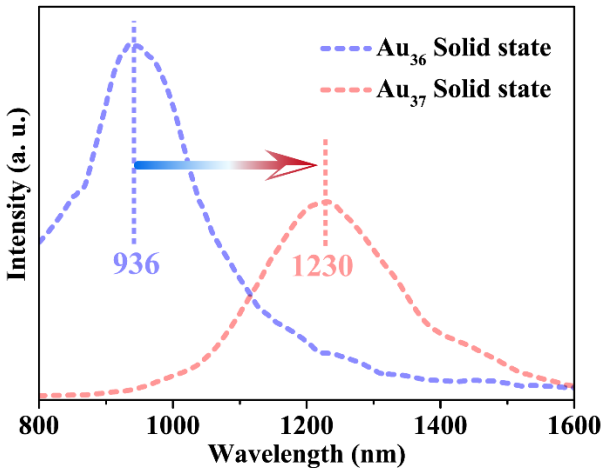

Figure S9. Near-infrared fluorescence spectra of solids of Au_{36} and Au_{37} nanoclusters.

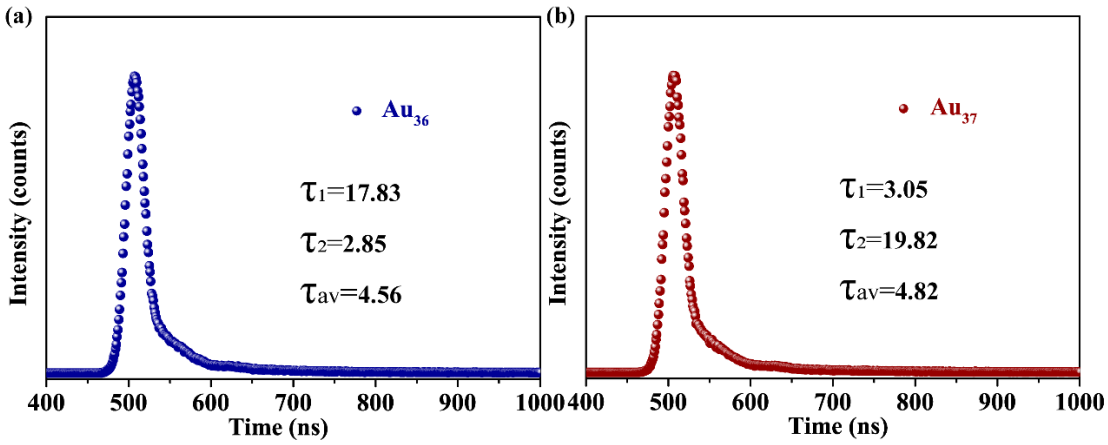

Figure S10. Near-infrared fluorescence lifetime spectra of solids of (a) Au_{36} and (b) Au_{37} nanoclusters.

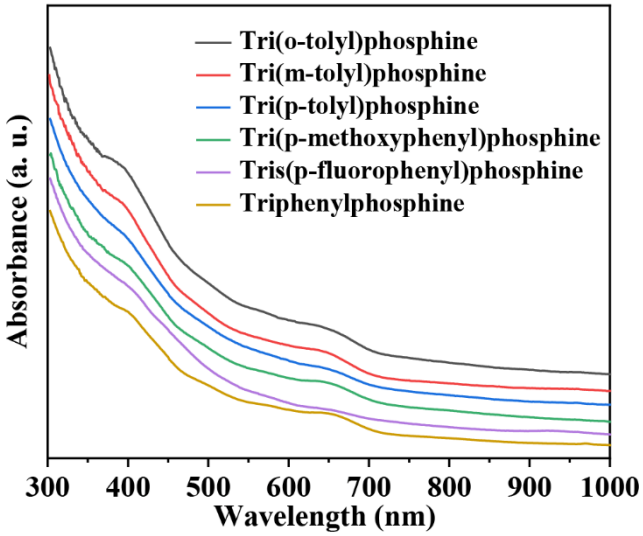

Figure S11. Au_{37} nanocluster protected by different phosphine ligands.

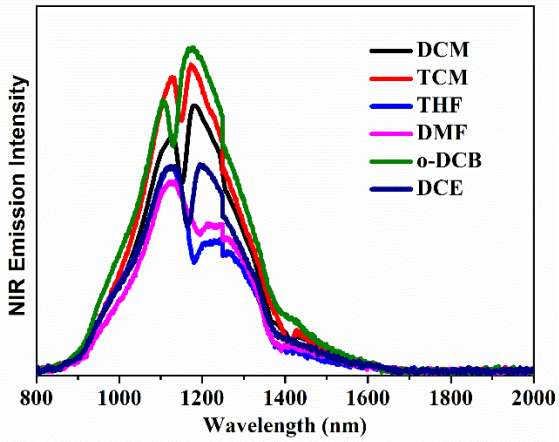

Figure S12. Intensity spectra of near infrared emission peaks of Au_{37} nanocluster in different solvents.

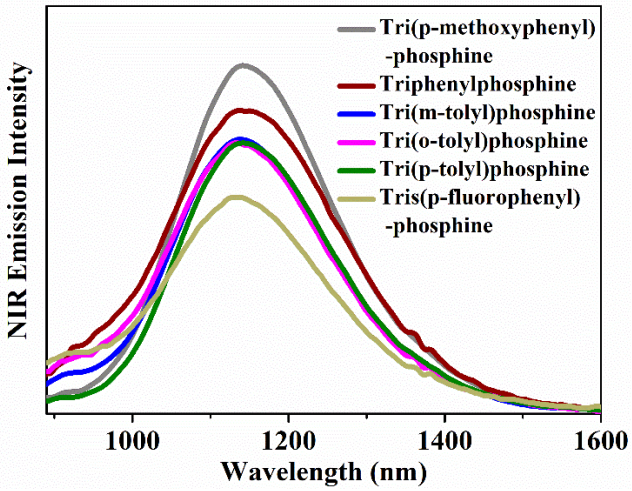

Figure S13. Intensity spectra of near infrared emission peaks of Au_{37} nanocluster for phosphine ligands with different substituents.

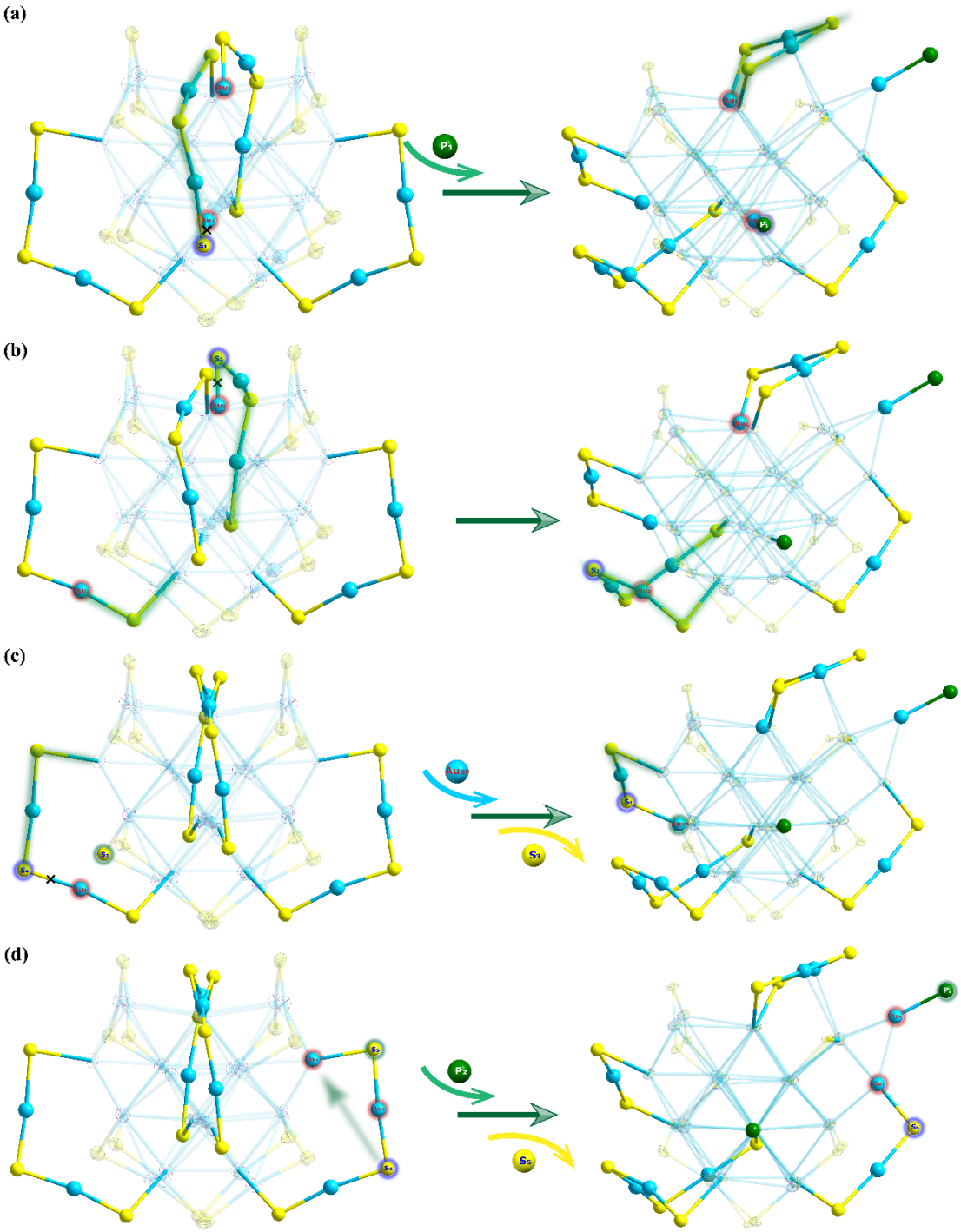

Figure S14. Possible steps of structural transformation from Au_{36} to Au_{37} nanoclusters.

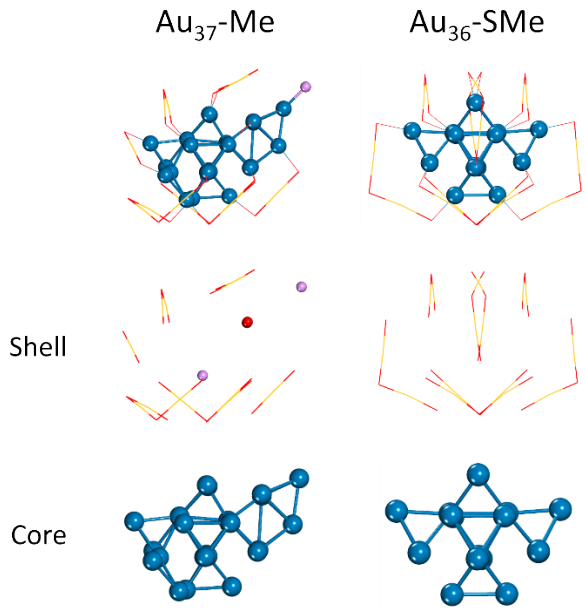

Figure S15. Fragment Definition of Au_{36} and Au_{37}.

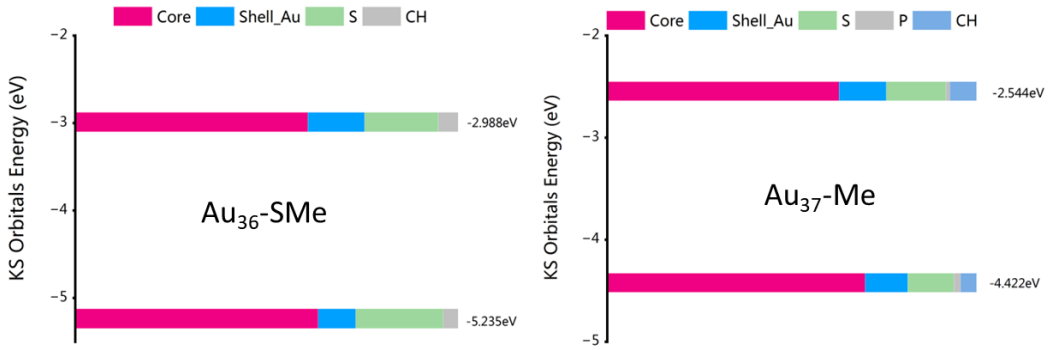

Figure S16. Contribution of phosphine ligands to emission.

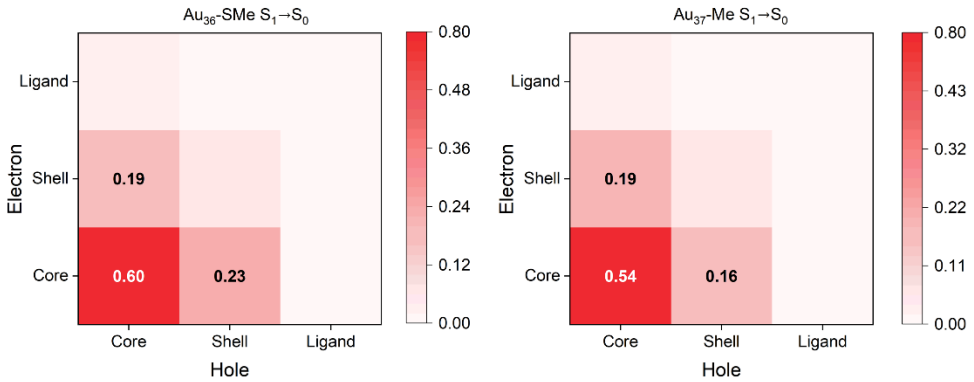

Figure S17. The charge transfer heat map by IFCT Analysis.

Table S1 Emission wavelengths of nanoclusters with NIR emission.

Nanoclusters in the NIR	Wavelength position (nm)
$Au_{18}(S\text{-}c\text{-}C_6H_{11})_{14}$ [10]	922
$Au_{25}(PET)_{18}$ [11,12]	949
$Au_{36}(TBBT)_{24}$ [13]	972
$[Au_{37}(PPh_3)_{10}(SC_2H_4Ph)_{10}Cl_2^+]$ [14]	1520
$Cu_{16}Pd_1L_{10}(PPh_3)_2(Pz)_6$ [15]	928
$Au_{44}[CH_3O(CH_3)_2C{\equiv}C]_{16}(C_6H_5)_6(tht)_2{\cdot}CH_2Cl_2{\cdot}H_2O$ [16]	958
$Au_{21}(S\text{-}Adm)_{15}$ [17]	820
$Au_{39}(PET)_{29}$ [18]	915
$[Cu_{31}(4\text{-}MeO\text{-}PhC{\equiv}C)_{21}(dppe)_3](ClO_4)_2$ [19]	1250
$Na_3[Ag_{29}(BDT)_{12}(TPP)_4]$ [20]	770
$Au_{52}(p\text{-}MBT)_{32}$ [21]	899
$Au_{25}(Capt)_{18}^-$ [22]	808
…	…
$Au_{37}(TBBT)_{21}(TPP)_2$	1152 (this work)

Table S2 Crystal data and structure refinement for $Au_{37}(TBBT)_{21}(TPP)_2$.

CCDC	2269529
Empirical formula	$C_{246}H_{303}Au_{37}P_2S_{21}$
Formula weight	11282.83
Temperature/K	120
Crystal system	triclinic
Space group	P-1
a/Å	23.9232(3)
b/Å	26.5335(4)
c/Å	26.9468(4)
α/°	107.8730(10)
β/°	94.1630(10)
γ/°	99.0720(10)
Volume/Å^3	15942.0(4)
Z	2
ρ_{calc}g/cm^3	2.350
μ/mm^{-1}	32.740
F(000)	10136.0
Radiation	Cu Kα (λ = 1.54186)
2Θ range for data collection/°	8.83 to 130
Index ranges	-25 ≤ h ≤ 28, -31 ≤ k ≤ 18, -31 ≤ l ≤ 30
Reflections collected	109906
Independent reflections	52549 [R_{int} = 0.0637, R_{sigma} = 0.1014]
Data/restraints/parameters	52549/2054/2712
Goodness-of-fit on F^2	0.900

Final R indexes [I>=2σ (I)]	R_1 = 0.0538, wR_2 = 0.1370
Final R indexes [all data]	R_1 = 0.0778, wR_2 = 0.1448
Largest diff. peak/hole / e Å^{-3}	3.26/-2.92

References

[1] C. Zeng, H. Qian, T. Li, G. Li, N. L. Rosi, B. Yoon, R. N. Barnett, R. L. Whetten, U. Landman, R. Jin, *Angew. Chem. Int. Ed.* 2012, **51**, 13114-13118.

[2] F. Neese, *WIREs Comput Mol Sci*, 2012**, 2**, 73-78.

[3] C. Adamo, V. Barone, *J. Chem. Phys.* 1999**, 110**, 6158-6170.

[4] F. Weigend, *Phys. Chem. Chem. Phys.* 2006**, 8**, 1057-1065.

[5] M. J. Frisch, et al., Gaussian 09 Revision A.1. Gaussian Inc. 2009.

[6] T. Lu, Multiwfn Manual, version 3.6(dev), Section 3.21.1 and 3.21.8, available at http://sobereva.com/multiwfn.

[7] Z. Liu, T. Lu, Q. Chen, *Carbon* 2020**, 165**, 461-467.

[8] T. Lu, F. Chen, J. *Comput. Chem.* 2012, **33**, 580-592

[9] Q. Li, C. J. Zeman IV, Z. Ma, G. C. Schatz, X. Wendy Gu, *Small* 2021, **17**, 2007992.

[10] S. Chen, S. Wang, J. Zhong, Y. Song, J. Zhang, H. Sheng, Y. Pei, M. Zhu, *Angew. Chem. Int. Ed*. 2015, **54**, 3145-3149.

[11] M. Zhu, E. Lanni, N. Garg, M. E. Bier, and R. Jin, *J. Am. Chem. Soc.* 2008, **130**, 1138-1139.

[12] M. W. Heaven, A. Dass, P. S. White, K. M. Holt, R. W. Murray, *J. Am. Chem. Soc.* 2008, **130**, 3754-3755.

[13] C. Zeng, H. Qian, T. Li, G. Li, N. L. Rosi, B. Yoon, R. N. Barnett, R. L. Whetten, U. Landman, R. Jin, *Angew. Chem. Int. Ed.* 2012, **51**, 13114-13118.

[14] Q. Li, C. J. Zeman IV, Z. Ma, G. C. Schatz, X. W. Gu, *Small* 2021, **17**, 2007992.

[15] S. Peng, H. Yang, D. Luo, G. Ning, D. Li, *Small* 2024, **20**, 2306863.

[16] W. Si, C. Zhang, M. Zhou, Z. Wang, L. Feng, C. Tung, D. Sun, *Sci. Adv.* 2024, **10**, eadm6928.

[17] Q. Li, C. J. Zeman IV, G. C. Schatz, X. W. Gu, *ACS Nano* 2021, **15**, 10, 16095-16105.

[18] Z. Liu, L. Luo, J. Kong, E. Kahng, M. Zhou, R. Jin, *Nanoscale* 2024, **16**, 7419-7426.

[19] T. Jia, Z. Guan, C. Zhang, X. Zhu, Y. Chen, Q. Zhang, Y. Yang, D. Sun, *J. Am. Chem. Soc.* 2023, **145**, 10355-10363.

[20] W. Ishii, Y. Okayasu, Y. Kobayashi, R. Tanaka, S. Katao, Y. Nishikawa, T. Kawai, T. Nakashima, *J . Am. Chem. Soc.* 2023, **145**, 11236-11244.

[21] Y. Wang, Z. Liu, A. Mazumder, C. G. Gianopoulos, K. Kirschbaum, L. A. Peteanu, R. Jin, *J. Am. Chem. Soc.* 2023, **145**, 26328-26338.

[22] F. He, G. Yang, P. Yang, Y. Yu, R. Lv, C. Li, Y. Dai, S. Gai, J. Lin, *Adv. Funct. Mater.* 2015, **25**, 3966-3976.